Acta Astronautica Vol. 15, No. 6/7, pp. 421–433, 1987
Printed in Great Britain

0094-5767/87 $3.00 + 0.00
Pergamon Journals Ltd

INITIAL ATTITUDE DETERMINATION FOR THE HIPPARCOS SATELLITE†

JOZEF C. VAN DER HA
European Space Operations Centre (ESOC), Robert-Bosch-Str. 5, 6100 Darmstadt, F.R.G.

(*Received* 6 *January* 1987)

Abstract—The present paper described the strategy and algorithms used during the initial on-ground three-axes attitude determination of ESA's astrometry satellite HIPPARCOS. The estimation is performed using calculated crossing times of identified stars over the Star Mapper's vertical and inclined slit systems as well as outputs from a set of rate-integrating gyros. Valid star transits in either of the two fields of view are expected to occur in average about every 30 s whereas the gyros are sampled at about 1 Hz. The state vector to be estimated consists of the three angles, three rates and three gyro drift rate components. Simulations have shown that convergence of the estimator is established within about 10 min and that the accuracies achieved are in the order of a few arcsec for the angles and a few milliarcsec per s for the rates. These stringent accuracies are in fact required for initialisation of subsequent autonomous on-board real-time attitude determination.

1. INTRODUCTION

ESA's astrometry satellite HIPPARCOS is planned to be launched into a geostationary orbit in mid 1988. Its primary objectives will be the systematic collection of star position measurements over its 2.5 year mission lifetime. After elaborate data processing these measurements will result in a star catalogue containing the positions, parallaxes, and proper motions of about 100,000 stars to an unprecedented accuracy in the order of 2 milli-arcsec and 2 milli-arcsec per year, respectively. HIPPARCOS' optical payload is equipped with two telescopes whose viewing directions are separated by 58 deg. Star images from both fields of view are superimposed onto a common focal plane by means of a beam combining mirror. In order to be able to execute the mission objectives a real-time on-board three-axes attitude pointing knowledge to an accuracy of as little as 1.0 arcsec (rms) is required. An overview of HIPPARCOS mission principles and objectives is found in [1].

During normal-mode operations attitude estimates are updated by the on-board computer about once per second using sampled gyro rate measurements providing three-axes attitude information. Star mapper signals are analysed to extract crossing instants of selected stars whose position coordinates have been uplinked to the on-board computer. Offsets between actual and expected crossing times are used for updating gyro drift estimates as well as the attitude state about once every 10 s in average, cf. algorithm in [2]. The on-board attitude estimation and Star Mapper sampling algorithms require an *a priori* attitude knowledge of an accuracy already at the arcsec level. It is thus evident that the initialisation of the on-board real-time attitude determination is far from straightforward and involves considerable ground support.

The present paper provides an outline of the strategy and algorithms used during the initial three-axes attitude determination performed on-ground using downlinked Star Mapper signals and gyro readings. At the time of Star Mapper initialisation the satellite is in Sun-Pointing Mode with its scan axis pointing within a cone of 1.6 deg semi-cone angle around the Sun direction and a scan rate (about its z-axis) of nominally 168.75 deg/h. No *a priori* scan angle knowledge is available. Gyro readings as well as the two (B and V filtered) Star Mapper streams which are sampled at 600 Hz are downlinked and are available for close to real-time ground processing. Bright stars (up to B magnitude 8 or 9) crossing the Star Mapper slits will be identified on-ground by a star pattern recognition algorithm, cf. [3]. Validated star transit times will be used in the estimation software. It is expected that identified stars will become available for attitude determination purposes about every 30 s in average. Star Mapper transits over the vertical slit system are utilised for updating estimates of the scan parameters (i.e. scan phase angle, scan rate and scan gyro drift rate). Star transits over the Star Mapper's inclined slit system will be combined with those over the vertical slits to provide a measurement of the star crossing elevation angle. This information is vital for updating the characteristics of the instantaneous scan plane described by the scan axis orientation angles, their rates of change and drift rates of the two active gyros with their input axes within the satellite's equatorial plane. It should be emphasized that the fact that there exist two fields of view (separated by 58 deg) allows a meaningful attitude determination since the Star Mapper measurements connect the spacecraft axes to two inertial

†Paper IAF-86-241 presented at the *37th Congress of the International Astronautical Federation*, Innsbruck, Austria, 4–11 October 1986.

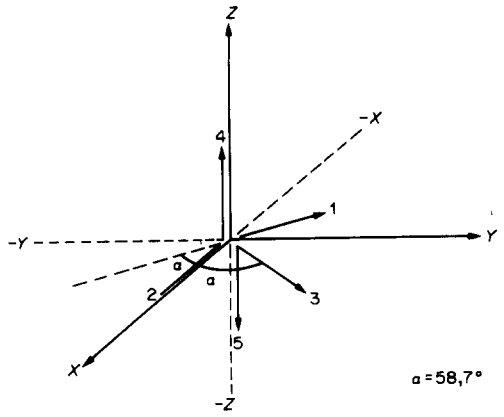

Fig. 1. Gyro input axes orientations within spacecraft reference frame (only 3 gyros are active at any time).

reference directions given by the star positions in the star catalogue. The star identification algorithm, however, is considerably complicated by the fact that stars from the two field of view directions are projected on the same focal surface. Finally, it is mentioned that in-between the occurrence of valid Star Mapper crossings attitude angles and rates can be derived from gyro rate measurements using latest available drift estimates.

2. GYRO SIGNAL CHARACTERISTICS

2.1. Gyro configuration and output model

The gyro input axes configuration adopted for HIPPARCOS is shown schematically in Fig. 1. Gyros 1, 2, 3 have their input axes within the spacecraft x, y plane: each combination of two gyros can be used and provides sufficient information for reconstituting the x and y rotation rates. The z-gyros 4 and 5 are fully redundant and only one will be used for establishing the rate about the z-axis. The nominal rate components during the initialisation phase are $\bar{\omega} = (0, 0, 168.75)$ deg/h.

The measured output corresponds to the observed rotation angle ΔG_k about each gyro's input axis during the sampling interval (t_{k-1}, t_k) of a little more than 1 s. From this angular measurement an estimate of the observed average rotation rate $\bar{g}_k$ over the interval Δt can be calculated immediately:

$$\bar{g}_k = \Delta G_k/\Delta t = \left\{\int_{t_{k-1}}^{t_k} g(t)\,\mathrm{d}t\right\}\Big/\Delta t, \quad k = 1, 2, \ldots \quad (1)$$

where $g(t)$ represents the output rate evolution in-between the sampling instants t_{k-1} and t_k. Naturally, the actual input rotation rate will be different from the result of eqn (1) because of gyro measurement errors. One may write:

$$\bar{g}_k = (1+\epsilon)\bar{\omega}_k + \bar{d}_k + \bar{m}_k + q_k, \quad (2)$$

where ϵ designates the scale factor error; $\bar{\omega}_k$ is the average of the actual rotation rate, $\bar{d}_k$ is the average gyro drift bias and $\bar{m}_k$ the averaged gyro rate noise, all over the relevant sampling interval. They are in fact defined in a similar manner as $\bar{g}_k$ in eqn (1) in terms of their instantaneous values. It is convenient in the present application to treat the scale factor term $\epsilon\bar{\omega}_k$ as part of the drift term, so it can be ignored here. The final noise term q_k represents quantisation noise. The resolution of the angular readings amounts to $9*10^{-6}$ deg which corresponds to a maximum quantisation error in the rate measurement of 0.015 deg/h. It can be shown that the effective quantisation error in the average rate over the average update interval is below 10^{-3} deg/h due to the fact that the quantisation error is retained in the integrator after sampling and is therefore incorporated in the following reading.

2.2. Gyro Noise Representation

The most important gyro output error sources in the present application are due to float torque noise (in range 10^{-2} to 1 Hz) and float torque derivative noise (below 10^{-2} Hz). The former effect is modelled as a zero-mean white noise $m(t)$ and the latter as a random walk, i.e. $\dot{d}(t) = n(t)$, with zero-mean white noise:

$$E\{m(t)m(\tau)\} = Q_m\delta(t-\tau),$$
$$E\{n(t)n(\tau)\} = Q_n\delta(t-\tau). \quad (3)$$

The PSD's (Power Spectral Densities) Q_m and Q_n of the random processes $m(t)$ and $n(t)$ over the relevant frequency range $f = 0.01$ to $f = 0.1$ Hz (corresponding to the range of update periods) are

$$Q_m(f) = 4*10^{-4} + (f-0.01)/150\ (deg/h)^2/Hz,$$
$$Q_n = 4*10^{-9}\ (deg/h/s)^2/Hz. \quad (4)$$

Because of thermoelastic distortions between the gyro package and the payload optics (of which the Star Mapper is a part) differential rates of significant magnitude are introduced which may be modelled as extra gyro drift noise. As long as the drifts are regularly updated by star transit information these distortions should not seriously affect the estimation accuracy. The PSD Q_n may need to be adjusted in order to properly reflect the effective drift rate variations.

The covariances of the rate and drift noises averaged over the update interval of length T can be calculated as:

$$\sigma_{\bar{m}}^2 = E(\bar{m}^{-2}) = E\left\{\int_0^T m(t)\,\mathrm{d}t\right\}^2\Big/T^2 = Q_m/T,$$

$$\sigma_{\bar{d}}^2 = E(\bar{d}^2) = E\left\{\int_0^T\left[\int_0^t n(\tau)\,\mathrm{d}\tau\right]\mathrm{d}t\right\}^2\Big/T^2 =$$
$$= Q_nT/3. \quad (5)$$

For update intervals between 10 and 100 s the rate noise $\sigma_{\bar{m}}$ would decrease from 0.01 to 0.002 deg/h whereas the average drift noise $\sigma_{\bar{d}}$ will increase from about 1 to $4*10^{-4}$ deg/h.

In comparison to rate noise the effects of quantisation and drift noise on the sampled rate mea-

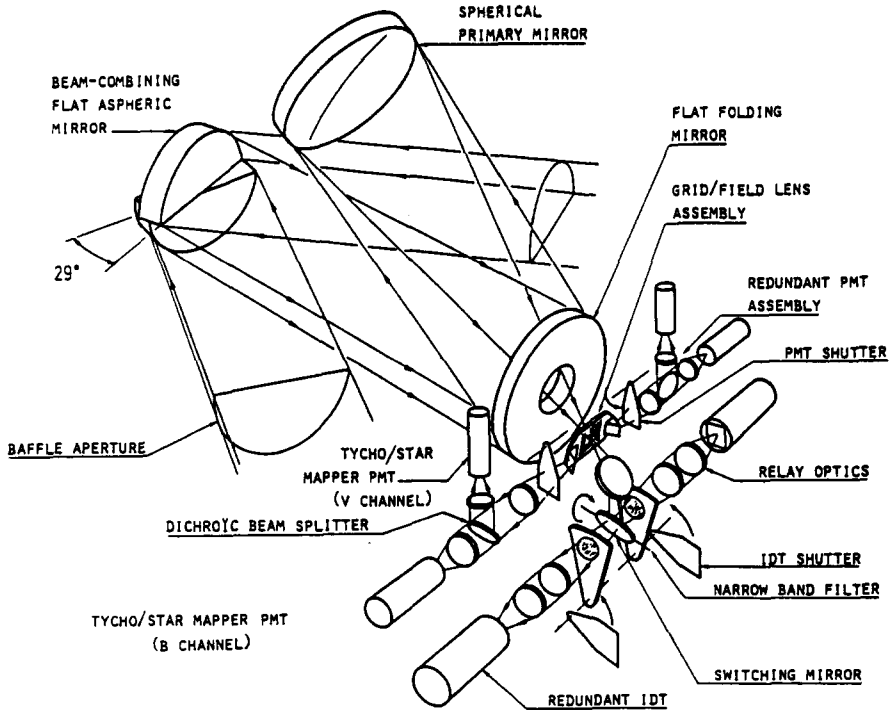

Fig. 2. HIPPARCOS payload configuration (PMT: photomultiplier tube; IDT: image dissector tube).

surements of eqn (2) can be ignored. Naturally, the long-term gyro drift variations must be included in the state estimation model, i.e. $\dot{d} = n(t)$ for each gyro, cf. eqns (3).

3. STAR MAPPER TRANSIT ANALYSIS

3.1. Description of Star Mapper

The HIPPARCOS Star Mapper is rather unique in the sense that it is not a conventional sensor unit but is entirely integrated into the optical payload used for the scientific data acquisition. Figure 2 provides an overview of the payload showing the two (redundant) Star Mapper assemblies. The light collected in the two telescopes is measured by the two operational photo-multipliers in different (B and V) spectral bands by means of a dichroic beam splitter. The photomultiplier detectors are sampled at a rate of 600 Hz and the resulting data streams are downlinked for ground processing.

Because of the imposed scanning motion the incoming light is modulated through the Star Mapper slit configurations. These are contained within the triangular areas on either side of the main modulating grid (which is used for primary scientific data collection) in the focal plane of the optical payload. The two Star Mapper configurations SM_1 and SM_2 (Fig. 3) are redundant but normally SM_1 will be used during the initialisation operations.

Each Star Mapper configuration consists of an opaque plate containing three groups of slits: the vertical slit system and the upper and lower inclined slit systems, cf. Fig. 4, extending ± 20 arcmin from the spacecraft equator. Each of the three slit systems consists actually of four non-equidistant slits. For analysis purposes a (virtual) reference slit midway between the two extreme slits is introduced. Star crossing times refer to the instants of passages over one of the three reference slits. In actual fact the modulated Star Mapper signal is subjected to a pre-determined matched filter adapted to the specific slit system characteristics. This results in a correlation peak at the instant when the star passes the virtual reference slit.

Since there are two telescope pointing directions each Star Mapper configuration has in fact six projected (virtual) slit systems on the celestial sphere as indicated in Fig. 5. The orientation of the reference slits of each of the six virtual slit systems within the spacecraft reference frame is described by the angles α_i, δ_i $(i = 1, \ldots, 6)$ defining the orientations of the normals $\underline{n}_i$ to the great circles containing the reference slits, cf. Fig. 6. The "sensitive" part of the Star Mapper slits is bounded by the angles $\mu_{i,\min}$ and $\mu_{i,\max}$. It can be seen that the angles α_i are approximately $\pm 29°$ and $\delta_i = 0$ or $\pm 45°$ depending on the slit system. The values for $\mu_{i,\min}$ and $\mu_{i,\max}$ are $(-20, 20)$ arcmin for the vertical slits and (0, 28.3) or $(-28.3, 0)$ arcmin for the inclined slits.

Finally, it should be emphasized that Star Mapper alignment errors may have a significant effect on the transit time analysis. The basic angle γ, i.e. angle between preceding and following field of view, may have an unknown bias of up to 5 arcsec which could be reduced to about 1 arcsec by in-flight calibration. In addition, there may be a grid rotation (about the

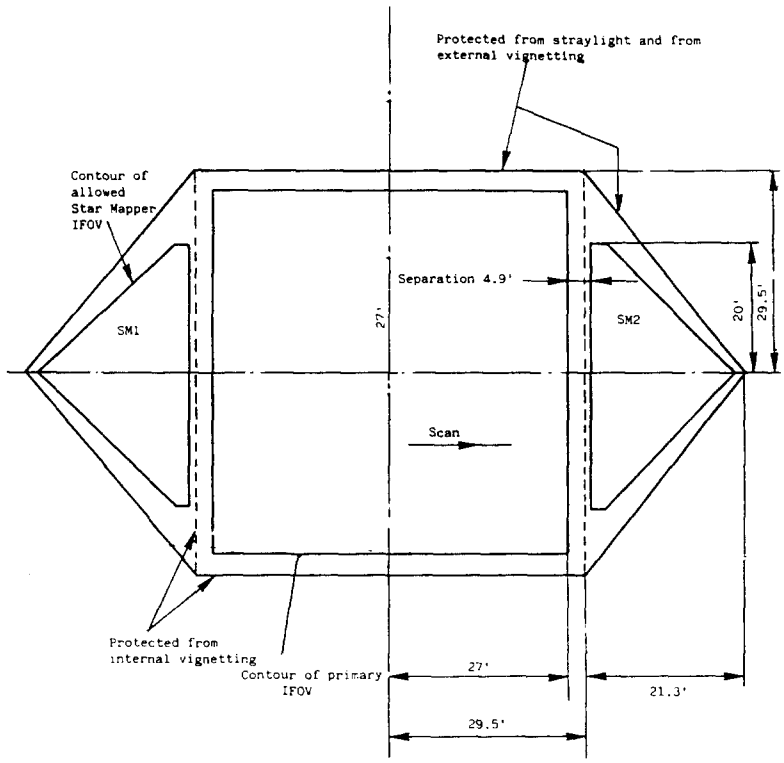

Fig. 3. Primary field of view and Star Mapper configuration.

optical axis) of up to 3 arcmin which would lead to a transit angle error of about 1 arcsec at the extremes of the Star Mapper slits.

3.2. *Derivation of crossing conditions*

During the Sun-pointing mode the spacecraft z-axis is controlled to remain pointing roughly in the Sun direction using angle information provided by a Sun Acquisition Sensor. It is expected that after on-ground calibration of the sensor bias angles the semi-cone depointing angle from the Sun will be below 0.6 deg.

The orientation of the spacecraft x, y, z frame relative to the adopted Sun-pointing reference frame X, Y, Z is described by the Tait-Bryan angles ϕ, θ, ψ, cf. Fig. 7:

$$\begin{pmatrix} \underline{x} \\ \underline{y} \\ \underline{z} \end{pmatrix} = [A(t)] \begin{pmatrix} \underline{X} \\ \underline{Y} \\ \underline{Z} \end{pmatrix}, \tag{6}$$

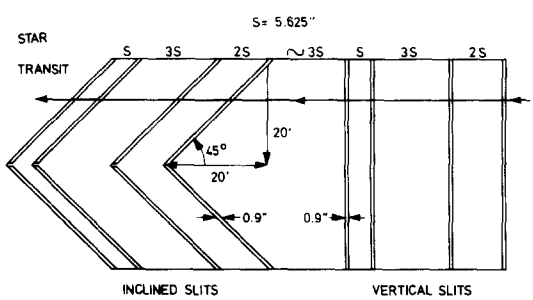

Fig 4. Star Mapper slit systems.

with components:

$$\begin{aligned}
a_{11} &= \cos\theta \cos\psi, \\
a_{12} &= \cos\phi \sin\psi + \sin\phi \sin\theta \cos\psi, \\
a_{13} &= \sin\phi \sin\psi - \cos\phi \sin\theta \cos\psi, \\
a_{21} &= -\cos\theta \sin\psi, \\
a_{22} &= \cos\phi \cos\psi - \sin\phi \sin\theta \sin\psi, \\
a_{23} &= \sin\phi \cos\psi + \cos\phi \sin\theta \sin\psi, \\
a_{31} &= \sin\theta, \\
a_{32} &= -\sin\phi \cos\theta, \\
a_{33} &= \cos\psi \cos\theta.
\end{aligned} \tag{7}$$

The normals $\underline{n}_i$ to the six (virtual) Star Mapper reference slits orientations in the spacecraft frame are denoted as follows:

$$\underline{n}_i = -\cos\delta_i \sin\alpha_i \underline{x} + \cos\delta_i \cos\alpha_i \underline{y} + \sin\delta_i \underline{z}. \tag{8}$$

The "slit reference frame" is completed by the unit-vectors $\underline{f}_i$, $\underline{g}_i$ as shown in Fig. 6:

$$\begin{aligned}
\underline{f}_i &= \cos\alpha_i \underline{x} + \sin\alpha_i \underline{y}, \\
\underline{g}_i &= \sin\delta_i \sin\alpha_i \underline{x} - \sin\delta_i \cos\alpha_i \underline{y} + \cos\delta_i \underline{z}.
\end{aligned} \tag{9}$$

The conditions which must be satisfied at the instant of a star transit over slit i may be expressed as:

$$\underline{n}_i \cdot \underline{s} = 0; \quad \sin\mu_{i,\min} < \underline{g}_i \cdot \underline{s} < \sin\mu_{i,\max}, \tag{10}$$

where $\underline{s}$ is the actual star position vector at the

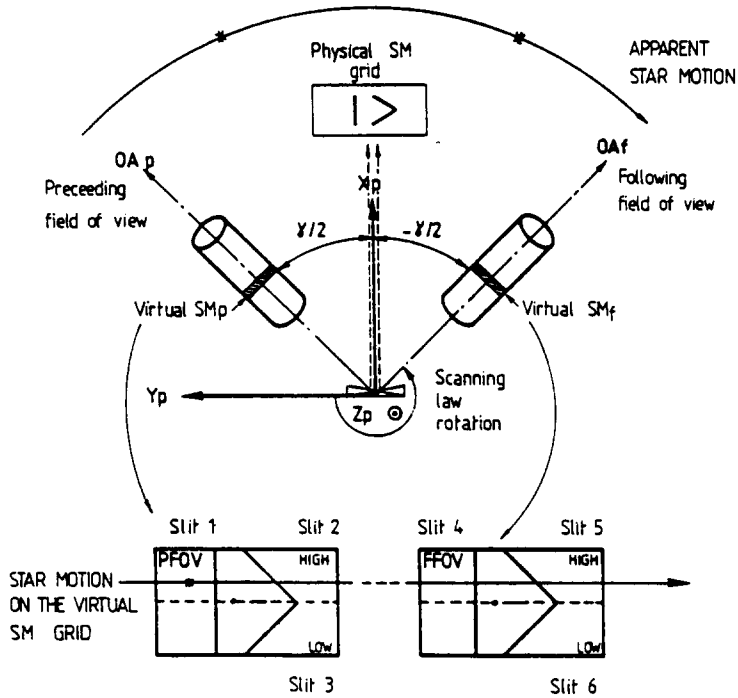

Fig. 5. Geometry of six virtual Star Mappel slit systems.

crossing instant. The first condition can most conveniently be analysed within the quasi-inertial Sun-pointing reference frame. The actual star position $\underline{s}$ is described by its right ascension and declination in this frame:

$$\underline{s} = s_1\underline{X} + s_2\underline{Y} + s_3\underline{Z} = \cos\alpha_s \cos\delta_s \underline{X} + \\ + \sin\alpha_s \cos\delta_s \underline{Y} + \sin\delta_s \underline{Z}. \quad (11)$$

With the aid of eqns (6) and (7) also the slit normal $\underline{n}_i$ can readily be expressed in the Sun-pointing frame. The first condition in eqns (10) can be written in explicit form as follows:

$$[B\cos\psi_i - A\sin\psi_i]\cos\delta_i + C\sin\delta_i = 0, \quad (12)$$

with the slit scan phase angle $\psi_i = \psi + \alpha_i$ and:

$$A = s_1\cos\theta + s_2\sin\phi\sin\theta - s_3\cos\phi\sin\theta,$$

$$B = s_2\cos\phi + s_3\sin\phi,$$

$$C = s_1\sin\theta - s_2\sin\phi\cos\theta + s_3\cos\phi\cos\theta. \quad (13)$$

A second equation is found from the second condition in eqns (10) using eqns (9) and (11):

$$[A\sin\psi_i - B\cos\psi_i]\sin\delta_i + C\cos\delta_i = \sin\mu_i, \quad (14)$$

where the crossing angle μ_i (cf. Fig. 6) between the star position and the slit's boresight direction $\underline{g}_i$ is defined by

$$\mu_i = \arcsin(\underline{g}_i \cdot \underline{s});\ \mu_{i,\min} \le \mu_i \le \mu_{i,\max}. \quad (15)$$

Combination of eqns (12) and (14) should lead to a solution for ψ_i and μ_i, i.e. the slit's boresight phase angle relative to the Sun-pointing X axis and the

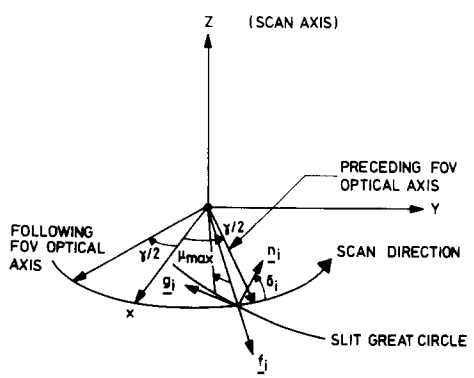

Fig. 6. Reference slit orientation in spacecraft frame.

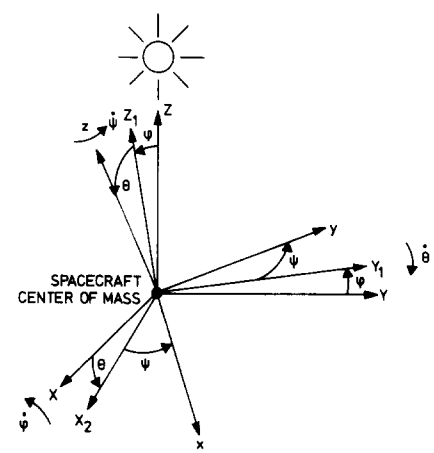

Fig. 7. Tait-Bryan angles ϕ, θ, ψ describing spacecraft frame relative to sun-pointing frame.

crossing angle along the slit plane. First, it is seen that:

$$A \sin\psi_i - B\cos\psi_i = \sin\delta_i \sin\mu_i,$$
$$C = \cos\delta_i \sin\mu_i, \quad (16)$$

which can be solved for ψ_i and μ_i:

$$\psi_i = \arctan(B/A) + \arcsin[\sin\delta_i \sin\mu_i / /(A^2 + B^2)^{1/2}],$$
$$\mu_i = \arcsin(C/\cos\delta_i). \quad (17)$$

These are exact results without approximations. For simplification of the final results a few reasonable approximations will be introduced:

(i) terms of order ϕ^4, $\phi^3\theta$, $\phi^2\theta^2$, θ^4 will be neglected as they are at the level of milliarcsec for worst-case depointing angle.

(ii) terms of order $s_3\phi^3$, $s_3^2\phi^2$, $s_3^3\phi$ (and similarly with θ) are also neglected as they are below 0.01 arcsec for maximum s_3.

(iii) terms of order μ_i^3 are neglected: these are of the order of 0.01 arcsec in the worst case.

With these assumptions the following explicit result for the crossing phase angle ψ_i can be derived:

$$\psi_i \cong \alpha_s + \Delta_s + \mu_i \cos\delta_i(\phi \cos\alpha_s + \theta \sin\alpha_s) + \mu_i \sin\delta_i \cos\delta_s, \quad (18)$$

with so-called depointing correction Δ_s given by:

$$\Delta_s = \tfrac{1}{4}(\phi^2 - \theta^2)\sin(2\alpha_s) - \phi\theta\cos^2\alpha_s. \quad (19)$$

This correction depends on the actual depointing angles and must be updated at each measurement instant using the latest available estimates of the scan plane orientation angles ϕ and θ. Its magnitude is up to 11.3 arcsec for maximum Sun-depointing of 0.6 deg. The latter two terms in eqn (18) have mean value zero for a star crossing the vertical slits. The first of these terms has a maximum amplitude of 12.6 arcsec and the second one of only 1.0 arcsec (under a maximum 3 arcmin grid rotation error) for vertical slit crossings.

3.3. *Measurement equations for vertical slits*

The general result established above in eqn (18) forms the basis for the measurement equations used in the state estimation process.

First, the vertical slit crossings are considered. These measurements provide knowledge on the scan phase angle and rate. In this case the slit orientation angle δ_i which would nominally be zero could be up to $\delta = 3$ arcmin due to the unknown grid rotation bias. Terms of order δ^2 however are below 0.2 arcsec and may be neglected. The general measurement equation expressing the slit's scan phase angle in terms of star catalogue positions follows from eqn (18):

$$\psi_i = \alpha_c + \Delta_s + \mu_i(\phi \cos\alpha_c + \theta \sin\alpha_c) + \delta\mu_i + \Delta\alpha_c, \quad (20)$$

where the actual star position α_s has been replaced by the catalogue value α_c plus an error $\Delta\alpha_c$ with covariance $E(\Delta\alpha_c^2) = (1.1 \text{ arcsec})^2$. Terms like $\mu_i\delta\ \delta_s^2$ are clearly negligible and have been omitted in eqn (20). It may be noted that for vertical slits the angle μ_i may be taken identical to the transverse offset ζ of the star's crossing relative to the spacecraft equator:

$$\zeta = \arcsin(\underline{s}\cdot\underline{z}) = \cos\delta \sin\mu_i \cong \mu_i \quad (i = 1, 4) \quad (21)$$

on the basis of present approximations.

It has already been stated that the depointing bias Δ_s will be calculated on the basis of the latest available ϕ, θ estimates. The terms $\delta\mu_i$ and $\Delta\alpha_c$ may be considered as random noise with a uniform probability distribution of worst-case amplitude of 1.0 arcsec for $\delta_i\mu_i$ and a Gaussian distribution with $\sigma_c = 1.1$ arcsec for the star position error along the scan plane, respectively.

The remaining term has a maximum value of $\mu_i\sqrt{(\phi^2 + \theta^2)}$ which is at most 12.6 arcsec for μ_i at the extremes of the slit. This term has a mean value zero as $E(\mu_i) = 0$ and could be modelled as a uniform probability distribution scaled by the latest estimate of the depointing angle. This noise however is rather large compared to other error sources. An improvement of this situation is offered by the fact that the actual absolute value of μ_i is indirectly known by comparing vertical and inclined slit transit times for the same star. It must be emphasized that due to the inclined slit ambiguity it is not known *a priori* whether the star crosses above or below the equator. The knowledge of the absolute value of ζ allows the covariance of the ψ measurement to be scaled according to the estimated Sun depointing angle:

$$\sigma_s^2 \leq E(\Delta\alpha_c^2) + \mu_i^2(\phi^2 + \theta^2) \leq (12.6 \text{ arcsec})^2. \quad (22)$$

The relatively insignificant error term $\delta\mu_i$ will be ignored. Star Mapper transit error sources induced by signal imperfections (due to defocusing and slit irregularities) are not significant and will be neglected for the present purpose. A further improvement in the noise covariance can be introduced when use is made of the fact that the sign of μ_i is known for crossings sufficiently far away from the equator, say 5 arcmin. In that case the third term in eqn (20) becomes a known bias just like Δ_s and can be corrected for. The noise reduces them to that due to *a priori* star position uncertainty and grid rotation. The noise model adopted will be eqn (22) when μ_i is less than 5 arcmin from the equator and $\sigma_s = 1.2$ arcsec otherwise.

3.4. *Measurement equations for inclined slits*

Inclined slit crossings provide knowledge on the scan plane orientation when they are used along with their corresponding vertical slit crossing: a measurement of the star's transverse position relative to the spacecraft equator is provided by the delay between the two crossings, cf. Fig. 4. The effect of transverse rates, however, must be accounted for. The

scan axis orientation is determined by the intersection of two cones (of semi-cone angle almost 90°) about the known star positions in each of the two fields of view.

The general result of eqn (16) becomes for inclined slits with nominal $\delta_i = \pm 45°$:

$$\psi_i \cong \alpha_c + \Delta_s + \tfrac{1}{2}\mu_i\sqrt{2}(\phi \cos\alpha_c + \theta \sin\alpha_c) + \\ + \mu_i \sin(\delta_i + \delta)\cos\delta_c + \Delta\alpha_c. \quad (23)$$

The angle δ is again the grid rotation angle of up to 3 arcmin whereas $\delta_i = \pm 45°$ depending on the slit identity. Note also that μ_i may be positive or negative with maximum value of 28.3 arcmin. Since the actual star right ascension α_s is the same for the vertical and inclined slit crossings eqns (20) and (23) provide the identity:

$$\alpha_s = \psi_1 - \Delta_s(t_1) - \zeta[\phi(t_1)\cos\alpha_c + \theta(t_1)\sin\alpha_c] - \delta\zeta \\ \equiv \psi_i - \Delta_s(t_i) - \tfrac{1}{2}\mu_i\sqrt{2}[\phi(t_i)\cos\alpha_c + \\ + \theta(t_i)\sin\alpha_c] - \mu_i \sin(\delta_i + \delta)\cos\delta_c. \quad (24)$$

Here i refers to an inclined slit ($i = 2, 3$) and use is made of eqn (21). Similar results are valid for ψ_4 and ψ_i ($i = 5, 6$). The variation of the depointing correction $\Delta_s(t)$ over the interval of time between the inclined and vertical slit crossings (which is less than 7.6 s) can be estimated using eqn (19). This difference turns out to be always less than 0.3 arcsec for maximum rates of 3 arcsec per s and will be neglected.

Similarly it can be shown that the terms introduced by variations in $\phi(t)$ and $\theta(t)$ are negligible. For inclined slits the star's transverse offset position from the spacecraft equator is given by:

$$\zeta = \cos(\delta_i + \delta)\sin\mu_i \cong \tfrac{1}{2}\sqrt{2}\,\mu_i \begin{cases}(1+\delta) & (i=2)\\ (1-\delta) & (i=3)\end{cases} \quad (25)$$

with an error of at most 0.1 arcsec.

With these preliminaries the following scan phase differences between inclined and vertical slits can be established from eqn (24):

$$\psi_i - \psi_1 \cong \mu_i \sin(\delta_i + \delta)\cos\delta_c - \delta\zeta \cong \\ \cong \zeta \cos\delta_c \begin{cases}(\delta - 1) & (i=2)\\ (1+\delta) & (i=3)\end{cases}. \quad (26)$$

It is noted that the rotation angle $\psi_i - \psi_1$ consists of a fixed part due to differences in slit intersection azimuth on the spacecraft equator (i.e. $\alpha_i - \alpha_1$) and the actual scan phase difference $\omega_z(t_i - t_1)$ with ω_z known from the latest scan rate estimation. Therefore, the measurement ζ is nominally given by

$$\zeta = \pm[\alpha_1 - \alpha_i - \omega_z(t_i - t_1)]/\cos\delta_c + \Delta\zeta, \\ i = 2, 3 \quad (27)$$

The numerical value of $\alpha_1 - \alpha_i$ is about 22 arcmin so that $\zeta >$, < 0 for $i = 2, 3$. The calculation of the bias term $\Delta\zeta$ is rather tedious as it contains also terms introduced by the change in slit azimuth under the grid rotation δ. It can be shown that $\Delta\zeta$ is given by:

$$\Delta\zeta = \begin{cases}-\delta(53' - \zeta), & (i=2)\\ \delta(53' + \zeta), & (i=3)\end{cases} \quad (28)$$

which means that $\Delta\zeta$ is at most ± 2.8 arcsec for a star crossing near $\zeta = 0$ and at most ± 1.7 arcsec for crossings near the extremes of the slits. Since the grid rotation is not known *a priori* these effects cannot be corrected for and will be incorporated in the measurement equations as extra random noise (note that mean value is zero).

The connection of the measurement ζ of eqn (27) with state parameters follows from eqn (21):

$$\zeta = s_1 \sin\theta - s_2 \sin\phi \cos\theta + \\ + s_3 \cos\phi \cos\theta + \Delta\zeta. \quad (29)$$

This can be reformulated in state-vector form:

$$\theta \cos\alpha_c - \phi \sin\alpha_c = (\zeta - \Delta\zeta - \Delta)/\cos\delta_c + \\ - \tan\delta_c - \Delta\delta_c, \quad (30)$$

with nonlinear depointing contribution:

$$\Delta = \tfrac{1}{6}\phi(\phi^2 + 3\theta^2)\sin\alpha_c - \tfrac{1}{6}\theta^3\cos\alpha_c + \\ - \tfrac{1}{2}\delta_c(\phi^2 + \theta^2). \quad (31)$$

The magnitude of Δ can be shown to be less than 0.2 arcsec so that Δ may be neglected. The remaining error terms $\Delta\zeta$ and $\Delta\delta_c$ may be combined as a Gaussian random noise with

$$\sigma_\zeta^2 = E(\Delta\zeta^2) + E(\Delta\delta_c^2) = (2.6 \text{ arcsec})^2. \quad (32)$$

This value will be taken as the measurement covariance during the state updating. In the measurement generation the actual biases, cf. eqn (28), will be used. Since terms of order $\zeta\delta_c^2$ are below 0.2 arcsec the final deterministic part of the measurement equation of eqn (30) may be reduced to:

$$\theta \cos\alpha_c - \phi \sin\alpha_c = \zeta - \tan\delta_c. \quad (33)$$

Finally, it should be emphasized that star crossings in the vicinity of the spacecraft equator (i.e. ζ near zero) cannot actually be used since there is a danger of assigning the wrong sign to ζ because of the slit ambiguity. From control law considerations it can be seen that stars with $|\zeta| < 5$ arcmin should be excluded from the update procedure. In fact, the noise for the remaining ζ measurements may then be reduced to 2.4 arcsec in eqn (32) since the grid rotation bias is less effective for larger values of ζ, cf. eqn (28).

4. STATE ESTIMATION MODEL

4.1. *Derivation of state model*

The state model describes the transition of the state parameters and their covariances in-between the mea-

surement instants. For ease of formulation the gyro readings are referred to the update instant when Star Mapper transits become available. The consequence is that higher frequency rate variations are averaged out. Naturally, these rates can be retrieved by processing the gyro measurements within the update interval. Gyro drift rates will be modelled as independent state variables to be estimated from the measurements.

The state vector adopted here is

$$\underline{x} = (\phi, \theta, \psi; \omega_x, \omega_y, \omega_z; d_1, d_2, d_3)^T, \quad (36)$$

with d_1, d_2 the drift rates of the two active equatorial gyros and d_3 that of the active z gyro. From the foregoing remarks it can be seen that the state evolution may be modelled by the linear system:

$$\dot{\underline{x}}(t) = H(t)\underline{x} + \underline{\tau}(t) + \underline{n}(t), \quad (37)$$

with 9×9 matrix $H(t)$ given by:

$$H = \left[\begin{array}{c|ccc|c} & \cos x_3/\cos x_2 & -\sin x_3/\cos x_2 & 0 & \\ 0 & \sin x_3 & \cos x_3 & 0 & 0 \\ & 0 & 0 & 1 & \\ \hline & 0 & a_x & 0 & \\ 0 & -a_y & 0 & 0 & 0 \\ & 0 & 0 & 0 & \\ \hline 0 & & 0 & & 0 \end{array}\right]. \quad (38)$$

The transformation between spacecraft frame and Sun-pointing reference frame has been given in eqns (6) and (7). Thus, the expression of body rates ω_x, ω_y, ω_z in terms of Tait-Bryan rates $\dot{\phi}$, $\dot{\theta}$ can readily be established. Inversion of these relationships results in:

$$\dot{\phi} = (\omega_x \cos\psi - \omega_y \sin\psi)/\cos\theta,$$

$$\dot{\theta} = \omega_x \sin\psi + \omega_y \cos\psi,$$

$$\dot{\psi} = \omega_z. \quad (34)$$

The body rates are obeying the well-known Euler equations which for the present application may be formulated as:

$$\dot{\omega}_x - a_x\omega_y = \tau_x,$$

$$\dot{\omega}_y + a_y\omega_x = \tau_y, \quad \dot{\omega}_z = \tau_z, \quad (35)$$

with "reduced" torque components τ_x, τ_y, τ_z in the range from $7*10^{-4}$ to $7*10^{-3}$ arcsec/s^2. The principal torque influence is provided by gyro reactions to the imposed scan rotation. Solar radiation, gravity-gradient and magnetic torques may be modelled as torque noise during the Sun-pointing phase. The Euler cross-coupling constants a_x and a_y are of the order of 38 and 13 arcsec/s, respectively, for the relevant parameters. An important aspect of the HIPPARCOS dynamical motion is the fact that the spacecraft reference axes are not principal axes. This dynamic imbalance of up to 3 deg introduces additional "inertial" torques of up to 10^{-3} arcsec/s^2 and up to a 10% change in a_x and a_y. As far as these effects cannot be included in the deterministic torque model they may be considered to be included in the system noise along with other model shortcomings.

The "torque" vector $\underline{\tau}$ obviously has only entries τ_x, τ_y, τ_z in row 4 to 6. This term contains the best available deterministic torque predictions and deviations from this model are represented by the noise terms n_4, n_5, n_6. Also the gyro drift noise is part of the system noise vector. All noise terms are described by their respective PSD's:

$$E\{n_j(t_1)n_j(t_2)\} = N_j\delta(t_1 - t_2), \quad j = 4, \ldots, 9. \quad (39)$$

On the basis of a 10% rate change after 100 s due to random torque variation imposed on a nominal acceleration of 10^{-3} for the equatorial rate and 10^{-4} arcsec per s^2 for the z-rate components, the following torque PSD's are obtained:

$$N_j = 10^{-6} \ (j = 4, 5); \quad N_6 = 10^{-8} \, (\text{deg/h/s})^2/\text{Hz}. \quad (40)$$

The gyro drift PSD's N_7 to N_8 have already been provided by Q_n in eqns (4).

4.2. *Discrete state model*

The continuous system given in eqn (37) is now discretised at the update instants t_k, $k = 1, 2, \ldots$ when Star Mapper crossing information becomes available. This results in the following system of difference equations:

$$\underline{x}_k = \Phi_k\underline{x}_{k-1} + \underline{u}_k + \underline{q}_k, \quad (k = 1, 2, \ldots) \quad (41)$$

with state transition matrix $\Phi_k = \Phi(t_k, t_{k-1})$. A sufficiently accurate representation of Φ_k is found by integrating the homogeneous part of eqn (37) while considering ϕ, θ, ω_x and ω_y equal to their initial

values over the update interval Δt_k

$$\Phi_k = \left[\begin{array}{c|ccc|c} & f_k\cos\psi_k/\cos\theta_k & -f_k\sin\psi_k/\cos\theta_k & 0 & \\ I & f_k\sin\psi_k & f_k\cos\psi_k & 0 & 0 \\ & 0 & 0 & \Delta t_k & \\ \hline & 1 & a_x\Delta t_k & 0 & \\ 0 & -a_y\Delta t_k & 1 & 0 & 0 \\ & 0 & 0 & 1 & \\ \hline 0 & & 0 & & I \end{array}\right] \tag{42}$$

with a "geometric factor" induced by the $\psi(t)$ variation:

$$f_k = 2\sin[\omega_z(t_k)\Delta t_k/2]/\omega_z(t_k) \quad (k = 1, 2, \ldots). \tag{43}$$

The forcing term $\underline{u}_k$ in eqn (41) can be calculated explicitly with the aid of the matrix superposition integral for a deterministic inhomogeneous system, cf. Gelb [4], Section 3.3:

$$u_k = \begin{bmatrix} \Delta t_k^2(\tau_x\cos\psi_k - \tau_y\sin\psi_k)/2 \\ \Delta t_k^2(\tau_x\sin\psi_k + \tau_y\cos\psi_k)/2 \\ \tau_k\Delta t_k^2/2 \\ \tau_x\Delta t_k + a_x\tau_y\Delta t_k^2/2 \\ \tau_y\Delta t_k - a_y\tau_x\Delta t_k^2/2 \\ \tau_z\Delta t_k \\ \underline{0} \end{bmatrix} . \quad (k = 1, 2, \ldots) \tag{44}$$

The torque contributions to the angle predictions are at most in the order of 13 arcsec per min whereas the corresponding rate changes amount to 0.4 deg/h over a one min interval.

Uncertainties in the torque model as well as errors induced by the dynamic imbalance and state model discretisation will be considered to be contained in the remaining noise term $\underline{q}_k$. This noise is assumed to be zero-mean and "white", i.e. realisations of $\underline{q}(t)$ at the instants t_{k-1} and t_k are presumed to be uncorrelated. The white noise $\underline{q}_k$ can be calculated using the matrix superposition integral:

$$\underline{q}_k = \int_{t_{k-1}}^{t_k} \Phi(t_k, \sigma)\underline{n}(\sigma)\mathrm{d}\sigma. \tag{45}$$

The covariance matrix $Q_k = E(\underline{q}_k \cdot \underline{q}_k^T)$ can readily be expressed in the PSD's $N_j (j = 4, \ldots, 9)$ of eqns (39) and (40):

$$Q_k = \int_{t_{k-1}}^{t_k} \Phi(t_k, \sigma)[N]\Phi^T(t_k, \sigma)\mathrm{d}\sigma, \quad (k = 1, 2, \ldots) \tag{46}$$

where $[N]$ is the diagonal matrix containing non-zero terms N_4 to N_9.

Using an approximate result for $\Phi(t_k, \sigma)$, namely $I + H_k(t_k - \sigma)$, it is possible to calculate the covariance matrix Q_k in explicit form:

$$Q_k = [N]\Delta t_k + [M]\Delta t_k^2/2 + [L]\Delta t_k^3/3, \tag{47}$$

with rather complicated matrices $[M]$, $[L]$ depending on N_j, $j = 4, \ldots, 6$; a_x, a_y and ψ_k, cf. Van der Ha [5]. It may be noted that although N_1 to N_3 are zero Q_1 to Q_3 contain non-zero entries because of integration of torque noise effects.

4.3. *Updates of state estimates*

The transition of the state estimate $\underline{x}_{k-1}^+$ (which is the result of the state updates performed at t_{k-1}) to $\underline{x}_k^-$, i.e. the best state estimate just before the updates at t_k are performed is given by eqn (41) with the random noise term $\underline{q}_k$ being omitted. The state covariance matrix must be adapted in order to account for the effect of the system noise covariance Q_k of eqn (47) over the interval t_{k-1}, t_k:

$$P_k^- = E\{\underline{x}_k^- \cdot \underline{x}_k^{-T}\} = \Phi_k P_{k-1}^+ \Phi_k^T + Q_k. \tag{48}$$

At the times t_k Star Mapper crossings and gyro rate readings become available for updating the state estimates. The formal star crossing measurement equations have the form:

$$\psi_m = \alpha_c - \alpha_1 + \Delta_s + m_\psi = [M_\psi]\underline{x},$$
$$\zeta_m = (\zeta - \Delta)/\cos\delta_c - \tan\delta_c + m_\zeta = [M_\zeta]\underline{x}, \tag{49}$$

with measurement matrices of eqns (20) and (30):

$$[M_\psi] = [0, 0, 1; 0, 0, 0; 0, 0, 0],$$
$$[M_\zeta] = [-\sin\alpha_c, \cos\alpha_c, 0; 0, 0, 0; 0, 0, 0], \tag{50}$$

and noise terms m_ψ, m_ζ with covariances as given in eqns (22) and (32), respectively.

The update of the state estimates at t_k is given by the wellknown Kalman filter:

$$\underline{x}_k^+ = \underline{x}_k^- + K_k(y_k - M_k\underline{x}_k^-), \tag{51}$$

with measurement $y_k = \psi_m$ or ζ_m and M_k the corresponding measurement matrix.

The Kalman gain matrix is defined as:

$$K_k = P_k^- M_k^T / \{M_k P_k^- M_k^T + \sigma_m^2\}, \quad (52)$$

where σ_m^2 is the relevant measurement noise covariance. Because of the fact that measurements are processed one by one (although at the same instant t_k) the term in the denominator of eqn (52) is a scalar, so no matrix inversion is required. The update of the state covariance matrix after the measurements have been processed in the state update is performed by a symmetric formulation:

$$P_k^+ = [I - K_k M_k] P_k^- [I - K_k M_k]^T + K_k K_k^T \sigma_m^2. \quad (53)$$

Gyro rate measurements g_j $(j = 1, 2, 3)$ from the three gyros in use will also be incorporated at the update instants t_k. Gyro rate measurements can be connected to state variables by means of the gyro projection matrix $[G]$ which expresses the transformation of body rates to gyro input axes (cf. Fig. 1) and depends on the identity of the active gyros:

$$\begin{pmatrix} g_1 \\ g_2 \\ g_3 \end{pmatrix} = \begin{pmatrix} d_1 \\ d_2 \\ d_3 \end{pmatrix} + [G] \begin{pmatrix} \omega_x \\ \omega_y \\ \omega_z \end{pmatrix} + \begin{pmatrix} m_1 \\ m_2 \\ m_3 \end{pmatrix}, \quad (54)$$

where the gyro rate noise m_j $(j = 1, 2, 3)$ can be expressed in the known noise PSD, cf. eqns (5). In state vector notation as in eqns (49) the gyro measurement matrices would become:

$$[M_j] = \begin{cases} [0, 0, 0;\ g_{j1}, g_{j2}, 0;\ 2 - j, j - 1, 0], & (j = 1, 2) \\ [0, 0, 0;\ 0, 0, 1;\ 0, 0, 1], & (j = 3) \end{cases} \quad (55)$$

where g_{ij} $(i, j = 1, 2)$ are the corresponding terms of the projection matrix [G]. The state and covariance updating due to gyro measurements can of course be carried out in the same manner as described above for the star transits, cf. eqns (51) and (53).

5. DISCUSSION OF RESULTS

The measurement and state estimation models have been implemented in software and a few of the simulation results will be presented here.

Initial state parameter values are selected within worst-case bounds from their nominal expected values, i.e. up to about 0.6 deg in the angles and up to 2 deg/h in the rates. Also larger discrepancies are acceptable as the estimator is not sensitive to the values of the initial estimates. A few different initial scan angles are selected as this angle governs the relative observability of the ϕ, θ angles according to the field of view in which the star transit occurs. Torque inputs are chosen on the basis of best available torque models. Bias values of up to 10% in torque values and Euler cross-coupling terms are considered here. The system noise covariances must be selected carefully with respect to these biases as they govern the weighting of incoming measurements with respect to the *a priori* state estimates based on the state transition model.

The interval in-between valid star crossings is selected to be 30 s. The intervals can optionally be taken as fixed or drawn from an interval distribution with expected value of 30 s. Transverse offsets and field of view of the star crossings are drawn from random number generators. Crossings within 5 arcmin of the satellite equator are discarded because of danger of a slit distinction error.

Figures 8a–c show the simulation results for a case without torque errors or biases. It is seen that convergence is essentially established after less than 10 min. It is of interest to point out that in the interval between 15 and 22 min the preceding field of view is drawn 12 times out of 14 trials. The degradation in the accuracy of ω_x over this interval is a consequence of the fact that the rotation angle about this axis (i.e. θ since ψ is near 90°) is almost unobservable over this interval. A comparison of accuracies with a case without torque influences at all has shown estimation errors of similar magnitude so it can be concluded that the state transition performs adequately. Also different star distributions were considered: these invariably lead to better accuracies so the distribution in Figs 8 may be considered to be rather unfavorable.

Figures 9a–c show the effects of torque estimation biases between 5 and 10% on all axes as well as on the Euler cross-coupling terms.

In comparison with Figs 8 it is seen that the angle estimates are slightly degraded. The convergence of the rates and gyro drifts is somewhat slower than before. The spike in ω_x at 32.5 min is caused by a thruster actuation where the covariance of the corresponding angular rate is relaxed by an amount equal to the expected rate change.

Figure 10 shows the estimation of the depointing angles when in addition to the torque biases a maximum grid rotation bias of 3 arcmin is introduced. It is seen that this bias has a significant influence on the accuracies especially in the region after 15 min where the star distribution is unfavorable. The rates appear not to be significantly affected by this bias.

Finally, Fig. 11 shows the estimation of the depointing angles for a variable update interval under the same conditions as in Fig. 9. A comparison shows no significant differences. It can be concluded that similar overall accuracies as for fixed intervals are achieved but slightly larger local excursions may occur.

6. CONCLUDING REMARKS

The measurement equations and state estimation model of HIPPARCOS initial attitude determination have been presented. The initial on-ground attitude reconstitution is required to reach an accuracy down to a few arcsec in order that the on-board autonomous attitude estimation can be initialised. Simu-

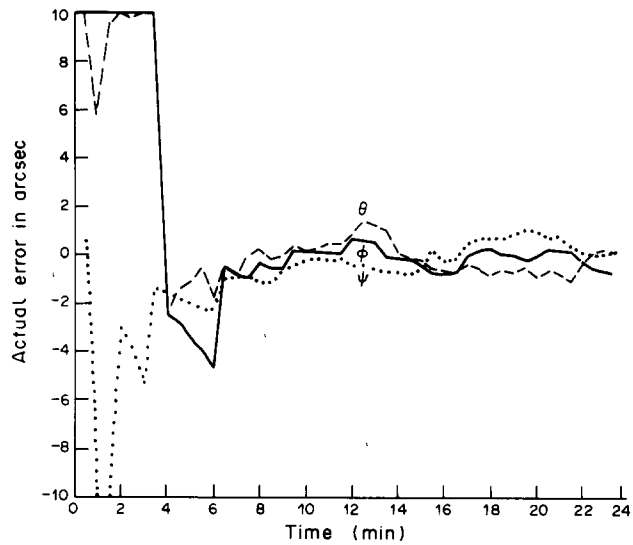

Fig. 8a. Attitude angle estimation.

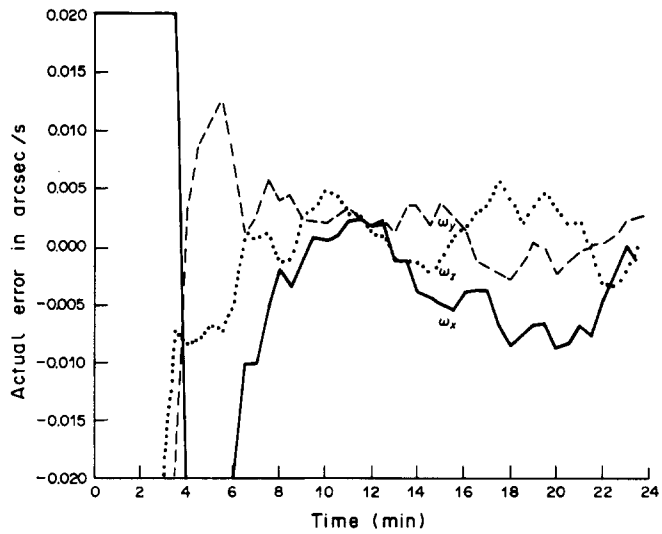

Fig. 8b. Attitude rate estimation.

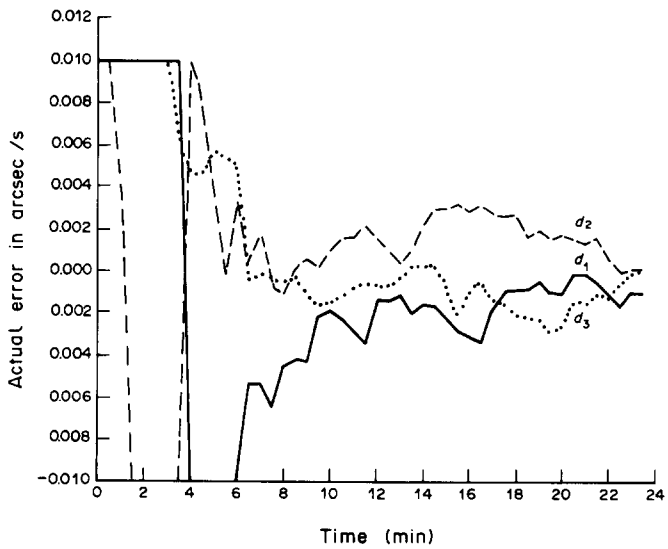

Fig. 8c. Gyro drift estimation.

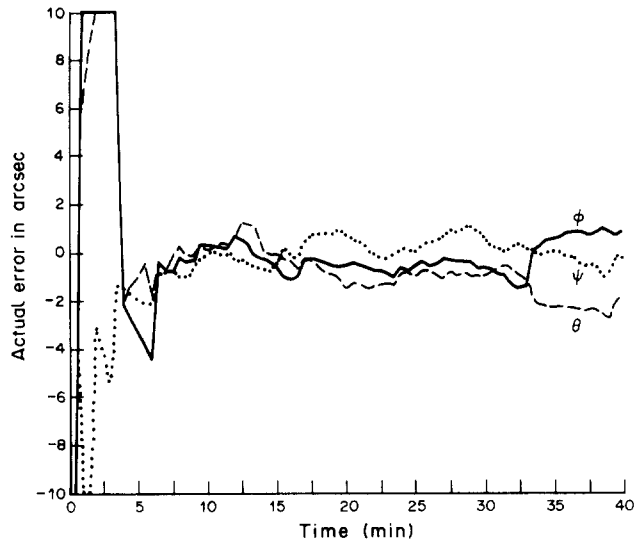

Fig. 9a. Attitude angle estimation.

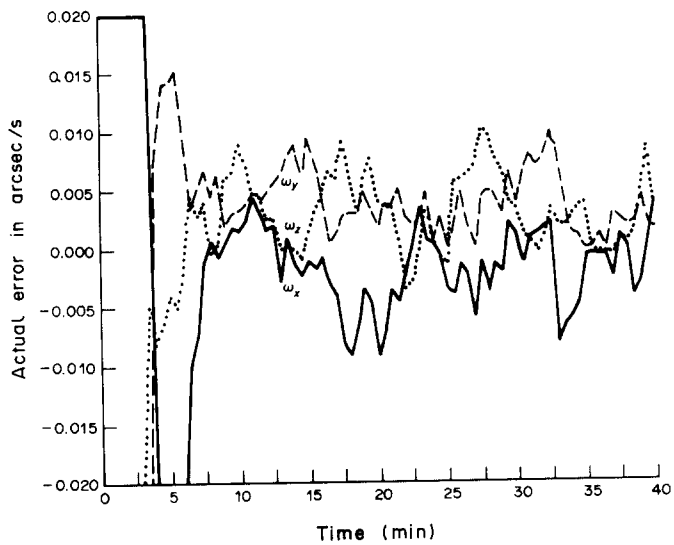

Fig. 9b. Attitude rate estimation.

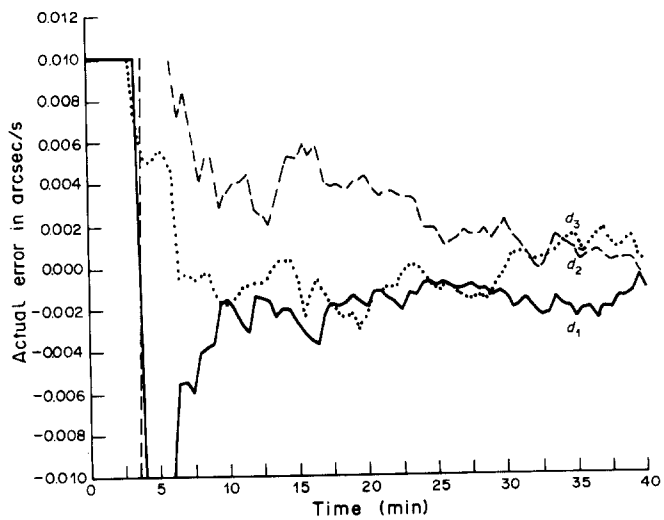

Fig. 9c. Gyro drift estimation.

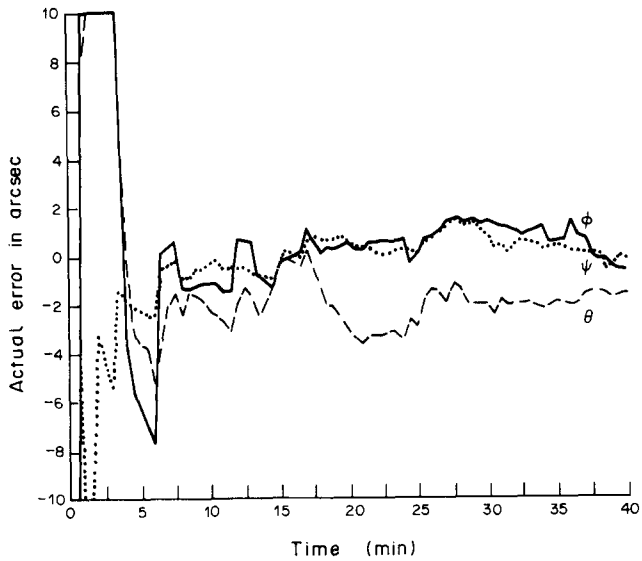

Fig. 10. Attitude angle estimation.

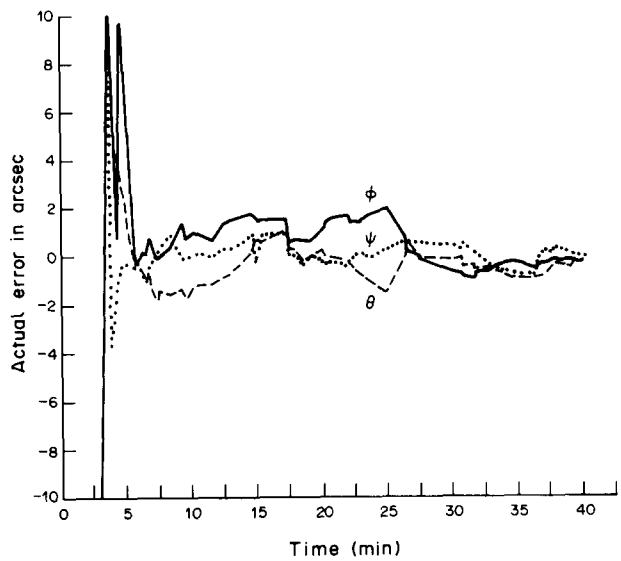

Fig. 11. Attitude angle evolution.

lations have shown that these accuracies can be reached on the basis of the model presented even in the presence of worst-case measurement biases induced by alignment errors, dynamic modelling shortcomings and star distribution variations. The simulations appear to indicate that alignment biases are the most significant input errors. Torque biases and actuation effects are relatively harmless provided that the system noise model is sufficiently realistic.

REFERENCES

1. M. Schuyer, HIPPARCOS—A European astrometry satellite: mission objectives, technical issues and approaches. In *Space 2000*, Edited by L. G. Napolitano, pp. 355–372. AIAA, New York (1983).
2. D. P. Vilain and R. S. Harris, Attitude determination and control of the HIPPARCOS satellite. In Guidance and Control 1984 (Edited by R. D. Culp and P. S Stafford), pp. 93–120. Univelt, San Diego (1984).
3. J. C. Van der Ha and S. P. Caldwell, HIPPARCOS precise attitude determination: a balance between on-board on on-ground capabilities. *Proceedings of the Second International Symposium on Spacecraft Flight Dynamics*, Darmstadt, F.R.G., ESA SP-255, pp. 385–393 (1986).
4. A. Gelb, *Applied Optimal Estimation*. MIT Press, Cambridge, U.S.A. (1974).
5. J. Van der Ha, HIPPARCOS fine attitude determination during initialisation phase. *OAD Working Paper No. 322*, ESOC, Darmstadt, F.R.G. (1986).